Thermal Conductivity, Second Sound, and Phonon-Phonon Interactions in NaF[†]

Howard E. Jackson and Charles T. Walker

Department of Physics, Northwestern University, Evanston, Illinois 60201

(Received 4 August 1970)

The thermal conductivity of several NaF crystals of varying purity has been measured between 2 and 100 °K. The full Callaway formalism is employed to derive phonon-phonon scattering rates from the thermal-conductivity data. The data can be fitted above 37 °K only by assuming a change from the low-temperature scattering rates. Heat-pulse data and the observation of second sound are reported for a crystal less pure than that studied by Jackson *et al.* The temperature region of second-sound propagation observed for several NaF crystals of varying purity along with the derived phonon-phonon scattering rates are used to give quantitative meaning to the criteria for the observation of second sound. The thermal-conductivity measurements and the second-sound observations are consistent with a scattering rate for normal processes between 10 and 25 °K of $\tau_N^{-1} = 1 \times 10^{-10} \, \omega T^4 \, \text{sec}^{-1}$.

I. INTRODUCTION

Direct measurements of the frequency and temperature dependence of phonon-phonon scattering rates are difficult to obtain. Ultrasonic attenuation experiments, while direct and monochromatic, have the disadvantage of being confined to frequencies below 10^{11} Hz.[1] Thus the thermal-phonon region is not readily accessible by this technique. Thermal-conductivity measurements, on the other hand, allow study of thermal phonons but have the disadvantage that one studies all phonons simultaneously. Extraction of phonon-phonon scattering rates from such data involves assumptions and averages over phonon spectra which leave one with less detailed information than one would like.

In recent years the technique of heat-pulse propagation has been developed.[2] Under certain conditions of temperature and crystal purity, one can, in fact, observe heat-pulse propagation with characteristics associated with the "second-sound" phenomenon so well known in liquid helium. In 1966, Ackermann *et al.*[3] observed second-sound propagation for the first time in a solid; in their case the solid was ^{4}He. This was followed in 1969 by observation of second sound in solid ^{3}He by Ackermann and Overton.[4] Finally, in 1970 McNelly *et al.*[5] observed what was called the "onset of second sound" in a conventional insulator, solid NaF. These latter results were confirmed and extended by Jackson, Walker, and McNelly.[6] Thus, there is little doubt that propagation of heat by thermal waves, with the characteristics of second sound, is a property of insulating solids.

The advantage of second-sound measurements is that they allow a reasonably direct determination both of the normal-process (*N*-process) phonon-phonon scattering rate and of the resistive-scattering rate as functions of temperature. A review article by Ackermann and Guyer[7] demonstrates this

for the case of solid ^{4}He.

The purpose of the present paper is to report the results and analysis of our thermal-conductivity and second-sound data on solid NaF. As will be seen, analysis of these two different sets of experiments allows one to extract complementary information about phonon scattering rates. The two together provide more confidence in the results than either separately.

NaF was chosen because both Na and F exist in nature with but one chemical isotope each. This means that resistive phonon scattering by the random isotopic mixture, common to most solids, is automatically absent. Second, one can obtain quite pure starting powder (~12-ppm cationic impurities), so conventional, if onerous, crystal purification techniques suffice for quite good final single crystals (~ 1 ppm). Thus, one can also reduce the resistive phonon scattering due to background chemical impurities to levels low enough to allow observation of second sound.

The rest of the paper is organized as follows: In Sec. II we detail the technique of crystal purification. In Sec. III we display our thermal-conductivity and heat-pulse data for several "pure" crystals of different purity. The heat-pulse data demonstrate transport by ballistic phonons, by second sound, and by diffusion. Section IV contains an outline of the theoretical ideas underlying an interpretation of the data. In Sec. V the theory is applied to the thermal-conductivity data to obtain estimates of phonon scattering rates, which are applied to the second-sound data in Sec. VI.

II. CRYSTAL PREPARATION

An extended multiple-growth technique was used to produce the ultrapure NaF single crystals. This technique employs repeated fractional recrystalization to lower the impurity content in the single-crystal growths. The technique was dictated since pu-

rification by ordinary zone refining for NaF is diffi-
cult due to its corrosive nature. To effect the re-
growth procedure, all of the crystals were grown
using the Kyropoulos seed-pulling technique in an
NRC model 284 crystal-growing furnace modified
to allow crucible handling under high vacuum. The
usual care was exercised in baking out the furnace
and especially the graphite parts, in using the fur-
nace exclusively for NaF growth, and in purifying
the ultrapure (Linde-4N6) argon-growth atmosphere.
The platinum crucibles were obtained from Matthey
Bishop, Inc.,[8] and have been used exclusively for
NaF growth.

To minimize water absorption and contamination
by OH⁻, extreme care was used in powder handling.
The starting powder was Merck "Suprapur."[9] It
was exposed only to purified He gas, purified Ar
gas, or vacuum. To charge the crucible, for in-
stance, a vacuum dry box was evacuated, backfilled
with high-purity dry He gas through a liquid-nitro-
gen-cooled activated-charcoal trap, loaded with the
crucible and powder through a port, reevacuated,
and finally backfilled again for the actual transfer
of powder to the crucible. In addition, the OH⁻
impurity was minimized by pumping on the furnace
before growth and while slowly warming the powder
to 650 °C. Above 650 °C, a one-third atmosphere
of carefully purified argon gas was admitted for the
growth process. The argon was purified by passage
through a dry-ice-acetone-cooled trap, followed by
passage over a zirconium-titanium getter at 550 °C,
followed by passage through a dry-ice-acetone-
cooled activated-charcoal trap.

The actual procedure for repeated fractional re-
crystalization is schematically illustrated in Fig. 1.
Each horizontal line represents a crucible; only the
first-growth column of crucibles is initially charged
with powder. Half the melt of crucible 1 is grown
and remelted into crucible 9. Similarly, half of

crucible 2 is grown and remelted into crucible 9.
The same process is repeated for crucibles 3, 4,
and 10. Then half of the melt of crucible 9 is
grown and remelted into crucible 13. Similarly,
half of crucible 10 is grown and remelted into
crucible 13. At this point, the furnace is briefly
opened in order to charge crucibles 5–8. The
entire procedure above is repeated until crucibles
14 was filled. Half the melt of both crucible 13
and 14 was grown and remelted into crucible 15.
Finally, the last (fourth) regrowth is pulled in its
entirety.

III. EXPERIMENTAL RESULTS

A. Thermal Conductivity

Thermal-conductivity-vs-temperature data for
the purest crystal are shown in Fig. 2. The sample
was sawed with a diamond string from the top of a
fourth-regrowth boule and sanded with 600-grit sand-
paper to 0.51×0.51-cm cross section. The sample
was then annealed for 40 h at a peak temperature of
950 °C. The peak thermal conductivity, a sensitive
indicator of impurity content, is seen to be 240 W/
°K cm. The position of the peak at 16.5 °K is to
be compared to crystals of lesser purity. Figure 3
shows thermal-conductivity-vs-temperature data
for several samples of differing purity. A typical
single growth from the Merck powder, for instance,
has a peak thermal conductivity of 58 W/°K cm at
only 13 °K. For a typical Harshaw NaF crystal, the
peak thermal conductivity of 30 W/°K cm occurs at
about 11 °K. The movement of the peak to higher
temperatures is evidence for the removal of the
Rayleigh-type impurity scattering and an approach
to a peak value determined solely by the intrinsic
phonon-phonon processes. The shape of the curve
in Fig. 2 emphasizes this point of view because we
see a very steep – in fact, exponential – dropoff
following the peak. This behavior was one of the
early predictions by Peierls[10] for umklapp-process
(U-process) scattering and is seen to some extent
in other insulating crystals of high purity.

B. Second Sound

In a recent paper we have reported on second-
sound propagation in our purest crystal.[6] Here we
wish to present results showing the effect of im-
purities on the second-sound mode. Figure 4 shows
heat pulses in a crystal whose peak thermal conduc-
tivity K_{peak} is 150 W/°K cm (curve B, Fig. 3). The
topmost trace (11 °K) shows well-defined longitudinal
and transverse first-sound peaks, and there appears
to be a slight shoulder on the decaying transverse
peak. By 13 °K, *three* peaks can be clearly iden-
tified, longitudinal and transverse first sound, and
second sound. By 14.5 °K, the second-sound pulse
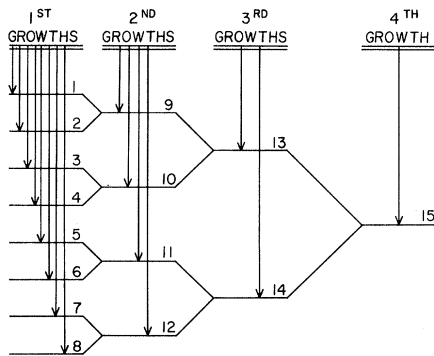is already superimposed on a broad diffusive ramp.

FIG. 1. Schematic illustration of crystal-growth
procedure. Each horizontal line represents a crucible,
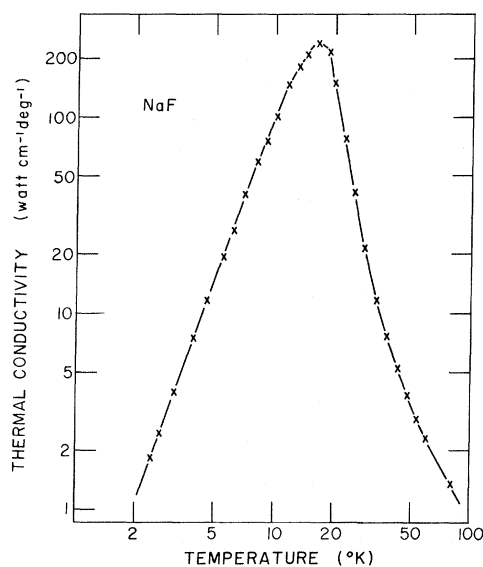each arrow a crystal growth.

FIG. 2. Thermal conductivity vs temperature for
purest NaF sample.

A plot of heat-pulse arrival time vs temperature
for this crystal is shown in Fig. 5. For the purpose
of discussion, a similar plot for our purest crystal
is reproduced in Fig. 6. In both instances one sees
ballistic longitudinal and transverse pulses at the
lowest temperatures; the second-sound pulse begins
to appear at 10 °K. In the less pure crystal, how-
ever, the second-sound pulse cannot be followed

FIG. 4. Heat pulses in a pure NaF sample ($l = 7.9$ mm)
in the $\langle 100 \rangle$ direction for several different temperatures.
L and T mark the peaks of the longitudinal and trans-
verse ballistic pulses, respectively. Note the appearance
of a third distinct pulse (second sound).

much past 14°K. In both figures the behavior at
highest temperatures is dominated by diffusion.
This difference between Figs. 5 and 6 shows the
extreme sensitivity of second-sound propagation to
background impurity content, since the impurity
content of the 150-W/°K cm crystal was only about
6 ppm in contrast to the ~1 ppm of the 240-W/°K cm
crystal.

A dramatic illustration of the effects of impurity
content is given by Fig. 7, where one sees a com-
parison of four different NaF crystals of varying
purity, two grown at Cornell University[11] (A and C)
and two grown at Northwestern University (B and
D). The data were taken at approximately the same
temperature and on samples of approximately
(within 10%) the same length, so that one may see
the effect of impurity content directly. In A (K_{peak}
$= 60$ W/°K cm) only longitudinal and transverse
ballistic pulses are seen, and the transverse pulse
is superimposed on a large diffusive ramp. In B
($K_{peak} = 150$ W/°K cm) one sees longitudinal and
transverse ballistic pulses and also a clearly sep-
arated second-sound pulse. In this case, the sec-
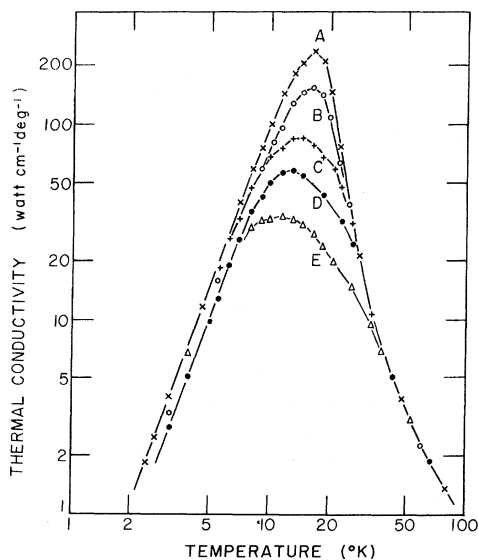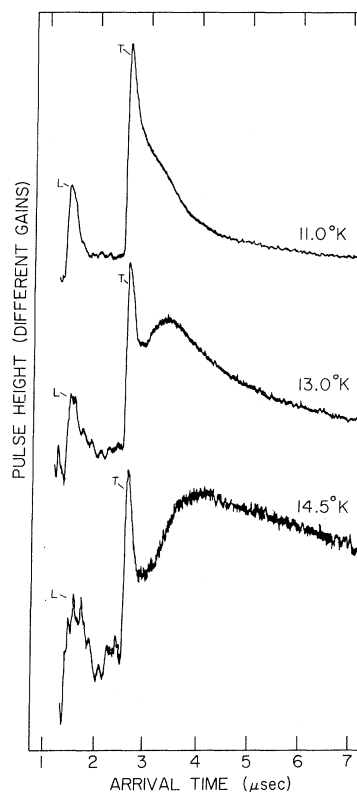ond-sound pulse has an amplitude somewhat less

FIG. 3. Thermal conductivity vs temperature for NaF
samples of varying purity: A, best fourth-regrowth sam-
ple; B, a less pure fourth-regrowth sample; C, best
single-growth sample; D, an average single-growth sam-
ple; E, best Harshaw sample.

FIG. 5. Arrival times vs temperature for leading edges and peaks of longitudinal ballistic pulse, the transverse ballistic pulse, and the second-sound pulse for the sample of Fig. 4.

than the transverse pulse amplitude. In both C ($K_{peak} = 150$ W/°K cm) and D ($K_{peak} = 240$ W/°K cm), the "transverse" pulse is considerably broadened and of greater relative intensity than the transverse pulses in A or B. In C, the signal does not quite return to the base line because of the diffusive background. Comparison of crystals A–D demonstrates
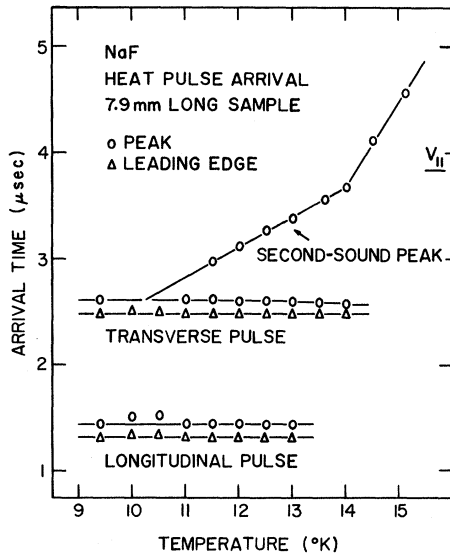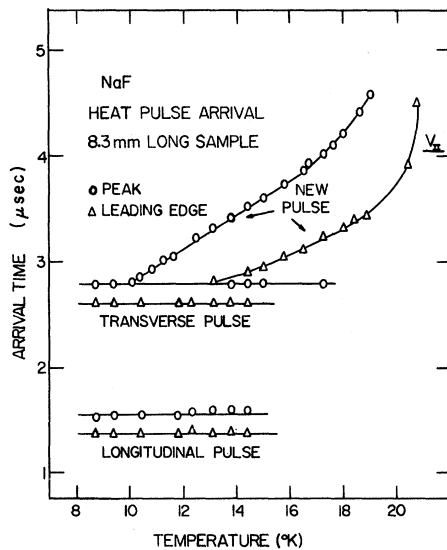
FIG. 6. Arrival times vs temperature for leading edges and peaks of longitudinal ballistic pulse, the transverse ballistic pulse, and the second-sound pulse for the purest sample. V_{II} is the expected arrival time for fully developed second sound.
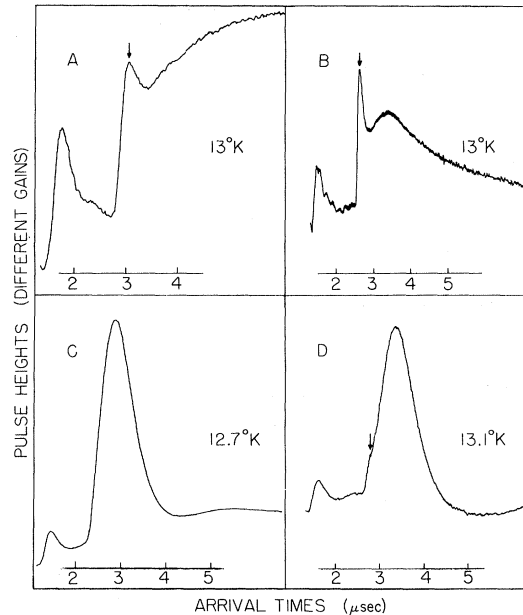
FIG. 7. Heat pulses in the ⟨100⟩ direction in four different NaF samples of varying impurity (A = 7.4 mm, B = 7.9 mm, C = 7.3 mm, D = 8.3 mm). The traces A–D are in order of increasing purity. Samples A and C were grown at Cornell University, and samples B and D at Northwestern University.

clearly that the purer the crystal, the greater the ratio of energy in the second-sound mode to the first-sound modes.

We shall now analyze the thermal-conductivity data in order to determine the temperature and frequency dependence of the phonon scattering rates. With these known we can see whether they are consistent with the second-sound data.

IV. THEORY

A. Thermal Conductivity

We shall use the phenomenological model of lattice thermal conductivity at low temperatures developed by Callaway.[12] Such a model is not, of course, developed from first principles, but its ability to describe the data has been well established.

Callaway's central contribution was his treatment of momentum-conserving or N processes in a crystal. N processes alone can be shown to lead to an infinite thermal conductivity. The N process, then, is quite different from U or impurity scattering processes which are momentum nonconserving and lead to a finite conductivity. The difference between momentum-conserving and non-momentum-conserving processes is reflected in the Boltzmann equation, which in the presence of temperature gradient is

$$\left(\frac{\partial N}{\partial t}\right)_c - \mathbf{c} \cdot \nabla T \frac{\partial N}{\partial T} = 0. \tag{1}$$

N is the phonon distribution function, c the phonon group velocity, T the temperature, and $(\partial N/\partial t)_c$ the rate of change of N due to collisions of any type. Callaway wrote the collision terms as

$$\left(\frac{\partial N}{\partial t}\right)_c = \frac{N(\vec{\lambda})}{\tau_N} + \frac{N_0 - N}{\tau_R}, \tag{2}$$

where τ_N is the relaxation time for N processes and τ_R the relaxation time for *all* non-momentum-conserving processes. Equation (2) shows that resistive processes relax the phonons to an equilibrium Planck distribution N_0 and that N processes relax the phonons to a *displaced* Planck distribution $N(\vec{\lambda})$. The separation of N and resistive processes leads to an expression for the thermal conductivity of the form

$$K = \frac{c^2}{2\pi^2} \int \tau_C \left(1 + \frac{\beta}{\tau_N}\right) C_{ph} k^2 dk, \tag{3}$$

where $\tau_C^{-1} = \tau_N^{-1} + \tau_R^{-1}$, C_{ph} is the phonon specific heat, and β is independent of the phonon wave vector k. The factor $1 + \beta/\tau_n$ is the "correction" caused by the special treatment of the N processes. Equation (3) may be written, using the Debye model, as the sum of two terms

$$K = K_1 + K_2,$$

where

$$K_1 = \left(\frac{k_B^4 T^3}{2\pi^2 c \hbar^3}\right) \int_0^{\Theta/T} \tau_C \frac{x^4 e^x}{(e^x - 1)^2} dx, \tag{4}$$

$$K_2 = \left(\frac{k_B^4 T^3}{2\pi^2 c \hbar^3}\right) \left(\int_0^{\Theta/T} \frac{\tau_C}{\tau_N} \frac{x^4 e^x}{(e^x - 1)^2} dx\right)^2 \Bigg/$$

$$\int_0^{\Theta/T} \frac{\tau_C}{\tau_N \tau_R} \frac{x^4 e^x}{(e^x - 1)^2} dx \ . \tag{5}$$

k_B is the Boltzmann constant, $x = \hbar\omega/kT$, and Θ is the Debye temperature. The same result has been more rigorously obtained by Krumhansl[13] as a special case of a general operator form of the Boltzmann equation.

For the usual case where resistive scattering dominates $(\tau_N \gg \tau_R)$, the correction term in Eq. (3), $1 + \beta/\tau_N$, becomes equal to 1 and the usual thermal-conductivity expression K_1 obtains. For the case of a very pure crystal, however, the N processes may dominate the distribution $(\tau_N \ll \tau_R)$ and we then find that the so-called correction term is the dominant term; that is, $K \to K_2$. A graph of the relative sizes of K_1 and K_2 for varying impurity content may be found in Ref. 14. If we look at the form of K_2, Eq. (5), we note that when N processes become infinitely frequent,

$$K \sim K_2 \to \frac{k_B}{2\pi^2 c} \left(\frac{k_B T}{\hbar}\right)^3 \left(\int_0^{\Theta/T} \frac{x^4 e^x}{(e^x - 1)^2} dx\right)^2 \Bigg/$$

$$\int_0^{\Theta/T} \tau_R^{-1} \frac{x^4 e^x}{(e^x - 1)^2} dx. \tag{6}$$

The expression then depends only on the *resistive* relaxation rate. In other words, one learns little of the exact strength or functional form of τ_N^{-1} from this term, but rather, one learns about τ_R^{-1}. Berman and Brock[14] were first to utilize this behavior to check the form and strength of τ_R^{-1} for isotope scattering by comparing the predictions of the full Callaway model to a fit of thermal-conductivity data for ^{6}LiF:^{7}LiF mixed crystals with a wide range of isotope concentrations. Only using the full Callaway model were they able to fit their data.

In order to fit the thermal-conductivity data, both the forms and strengths of all the phonon relaxation rates must be known. Namely, relaxation rates for N processes (τ_N^{-1}), U processes (τ_U^{-1}), boundary scattering (τ_B^{-1}), dislocation scattering (τ_D^{-1}), and impurity scattering (τ_I^{-1}) are needed. The strengths of the relaxation rates are not predicted theoretically for intrinsic processes and are somewhat uncertain for such extrinsic processes as dislocation scattering. There exist a number of functional forms for these processes, but with the exception of isotope or mass-difference scattering, these are not well confirmed experimentally. Furthermore, the functional forms for the intrinsic phonon relaxation rates change (presumably in a continuous fashion) as a function of temperature, and we must therefore decide whether a low-temperature functional form or a high-temperature form is appropriate for a particular temperature region.

B. Second Sound

The possibility of observing second sound in solids was first suggested by Peshkov in 1947.[15] In 1951, Ward and Wilks[16] considered a phenomenological Boltzmann equation to show that a density fluctuation in a phonon gas could propagate as a second-sound wave with velocity $V_{II} = c/\sqrt{3}$ (c = is the first-sound velocity). Subsequently, second sound has been placed on a much firmer theoretical footing by Guyer and Krumhansl,[17] and others,[18] using both semi-phenomenological and microscopic approaches. We shall use the Guyer-Krumhansl results for our brief discussion below.

The continuity equation for heat transport in an isotropic one-polarization Debye-model phonon gas is

$$C_v \frac{\partial T}{\partial t} + \vec{\nabla} \cdot \vec{q} = 0, \tag{7}$$

where C_v is the specific heat per unit volume and T is the temperature. In the phonon gas at low temperatures where the N-process mean free path λ_N is much shorter than the resistive mean free path λ_R, momentum conservation may be written

$$\frac{\partial \vec{q}}{\partial t} + \frac{c}{\lambda_R}\,\vec{q} + \tfrac{1}{3}C_v c^2\,\vec{\nabla}\,T - \tfrac{3}{5}\,c\lambda_N[\nabla^2 + 2\vec{\nabla}(\vec{\nabla}\cdot)]\,\vec{q} = 0.$$
(8)

If the N-process mean free path approaches zero, then one can combine Eqs. (7) and (8) to obtain a dissipative wave equation[19]:

$$\frac{\partial^2 T}{\partial t^2} + \frac{c}{\lambda_R}\,\frac{\partial T}{\partial t} + \tfrac{1}{3}\,c^2\,\nabla^2 T = 0.$$
(9)

If one has not only very frequent N processes but also very rare resistive processes ($\lambda_R \to \infty$), then we find that a temperature disturbance may propagate undamped with velocity $c/\sqrt{3}$. These ideas led to the following criteria for second-sound observation:

$$\lambda_N \ll \lambda \ll d,$$
(10)

$$\lambda_R \gg d,$$
(11)

$$\Delta t \ll d\sqrt{3}\,/c,$$
(12)

where λ is the second-sound wavelength ($\lambda \equiv 2\pi c/\Omega$), d is the sample thickness, and Δt is the heat-pulse duration. Equation (10) suggests that to have a collective propagation of phonons (the second sound), many N processes must occur within λ; and Eq. (11) suggests that if the temperature disturbance is to propagate as second sound, resistive processes which remove momentum from the second-sound pulse must not be present. It is crucial then that $\lambda_N \ll \lambda_R$, a condition that is obtained in a pure crystal at low temperatures. Second-sound data give a temperature range where these inequalities are satisfied and where they begin to fail. From these data, one may obtain a quantitative measure of the strengths of scattering processes.

If the conditions for second-sound propagation by heat pulses are satisfied, we may solve Eqs. (7) and (8) in the limit $\lambda_R \gg 1$ to find the shape of the detected pulse[7]:

$$T(l,\,t) = \frac{\Delta T}{6\pi}\,\Delta t\,e^{-t/2\tau_R}\,\frac{10\pi^{1/2}}{\tau_N t}\,\exp\frac{(l - V_{\mathrm{II}}\,t)^2}{\tfrac{6}{5}\,c^2\,\tau_N t}.$$
(13)

Consideration of the last term in Eq. (7) shows that as τ_N (or λ_N/c) becomes larger (fewer N processes), the pulse broadens. The broadening occurs because there are fewer N processes to keep phonons in the second-sound pulse; that is, the viscosity term of Eq. (8) is becoming effective. Using Eq. (13), then, one may analyze pulse broadening to determine a direct value of λ_N. Such an analysis has been carried out in detail for solid ^{4}He by Ackermann and Guyer.[7]

Finally, if conditions yet more stringent than those for second sound obtain

$$\lambda_N \ll R,$$
(14)

$$\lambda_N \lambda_R \gg R^2,$$
(15)

where R is the radius of sample and λ_R is the mean free path for momentum loss in the bulk of sample, then Poiseuille flow of phonons should be observed.[20] Phonons scatter via N processes to the walls where momentum loss occurs. In this case, the thermal conductivity exhibits a steep T^7-to-T^8 rise just before the peak value and may be represented[21] by

$$K = \tfrac{1}{3}\,C_v c^2\tfrac{5}{4}\,(R^2/c\lambda_N).$$
(16)

Thus far Poiseuille flow of phonons has been observed only in solid helium.[22] Such an observation gives a second direct measurement of λ_N.

V. DATA FITTING

We have investigated various theoretical fits to our thermal-conductivity data using the above full Callaway formalism. Our impurity content is low enough that the second integral (K_2) plays a dominant role in our fits. We have first fitted our purest-crystal data (Fig. 2) and then used these parameters to attempt a fit on the less-pure samples, changing only the strength of the impurity scattering.

Even with the uncertainties in strengths and functional forms of phonon relaxation processes mentioned above, a reasonable fit may be made to the data because different phonon relaxation rates dominate in different temperature regions. Below about 16 °K, the U scattering rate is insignificant compared to the other resistive processes. We have used calculated values of the boundary scattering rate τ_B^{-1} and the dislocation scattering rate τ_D^{-1} and an approximate value of the impurity scattering rate τ_I^{-1} to determine τ_N^{-1} for a good fit below 16 °K. We make use of the unusual behavior of K_2 [Eq. (5)] in this determination. We then add a U term for the fit above 16 °K. Above 35 °K, the fit breaks down as the relaxation times change their functional forms and new functional forms are substituted. We discuss each term in the relaxation rate next.

A. Extrinsic Process Scattering

1. Boundary Scattering

Since the original work of Casimir,[23] boundary scattering has been carefully investigated by Thatcher[24] and others and is well understood;

$$\tau_B^{-1} = c/1.12l$$
(17)

for a sample of square cross section, where l is a characteristic phonon mean free path limited by the boundaries of the sample and c is an averaged phonon velocity. We have used the average technique due to Slack.[25] A proper treatment of the averaged velocity would require separation into the longitudinal and transverse components as Holland[26] has done for germanium and silicon. No such attempt was made here. The calculated boundary scattering rate for a crystal size of 0. 51×0. 51 cm

is

$$\tau_B^{-1} = 7.0 \times 10^5 \text{ sec}^{-1}, \tag{18}$$

where a length correction of 15% according to Berman, Ziman, and Foster[27] is included. If τ_B^{-1} is regarded as a parameter whose value is found by fitting to the low-temperature data, one obtains

$$\tau_B^{-1} = 8.8 \times 10^5 \text{ sec}^{-1}, \tag{19}$$

in reasonable agreement with the prediction. Closer agreement between experiment and theory would require examination of the procedures used to obtain the average phonon group velocity. For instance, the difference between the theoretical and experimental values above would be reduced to 10% had we chosen the group velocity obtained by Houston's method.[28]

2. Dislocation Scattering

Dislocation scattering, in contradistinction to boundary scattering, is not so easily calculated with confidence. Theoretical attempts have been made by Klemens,[29] Carruthers,[30] and more recently by Ohasi.[31] Each obtains the form

$$\tau_D^{-1} = \Gamma_D N_0 \omega, \tag{20}$$

where N_0 is the dislocation density and Γ is the scattering strength. The values of the scattering strengths differ in these theories, all of them somewhat underestimating the experimentally observed strength. We shall use Ohashi's scattering strength because it is closest to past experimental values. We have observed the dislocation density directly in our samples using the etch of Davisson and Levine.[32] The etch-pit counts were made using a Leitz MM5 metallograph with oblique lighting. Since we did not wish to cleave in two the purest thermal-conductivity sample, we examined a number of crystals which had been grown and treated in the same manner as the purest thermal-conductivity sample. The random dislocation density in the interior of these samples varied from $5 \times 10^5/$cm^2 to a maximum of $1 \times 10^6/$cm^2. We shall see later that this dislocation density has a dramatic effect on the thermal conductivity of very pure crystals. For these dislocation densities, Ohashi's theory would predict

$$\tau^{-1} = 1.7 \times 10^{-8} \omega \text{ sec}^{-1}. \tag{21}$$

Using Γ_D as an adjustable parameter, the best data fit is obtained with

$$\tau_D^{-1} = 4 \times 10^{-8} \omega \text{ sec}^{-1}, \tag{22}$$

indicating that Ohashi's theoretical scattering strength, although a substantial improvement over Klemen's and Carruther's, is still too small.

3. Impurity Scattering

Before we can consider our central concern, the intrinsic phonon-phonon interactions, we must have a knowledge of the impurity scattering rate for our crystals. The choice of NaF for these experiments was intentional, for its natural isotopic purity eliminates a major impuritylike scattering mechanism. We are left, of course, with ordinary chemical impurity scattering. The starting powder was "guaranteed" to contain < 5-ppm Ca^{++}, < 5-ppm K^+, and < 12-ppm total.[33] The crystal-growth technique reduced the number of impurities to the 1-ppm level. At impurity concentrations on the order of ppm, standard laboratory techniques of impurity analysis become difficult. Consider, for example, infrared (ir) absorbtion, a standard technique for detecting OH^- impurity content. In NaF crystals, without any indication of OH^- from ir-absorbtion measurements, Harrison et al.[34] has found evidence from specific-heat anomalies implying a 0.1–0.3-ppm OH^- concentration. Even flame-emission spectroscopy becomes difficult unless one engages in high-purity wet chemistry. We may, however, utilize the results of ionic-conductivity measurements on our crystals[35] combined with the ionic-conductivity data on NaF of O'Brien and Plovnick.[36] O'Brien and Plovnick constructed an isothermal plot of ionic-conductivity vs divalent-impurity concentration obtained using a Jarrell-Ash emission spectrograph. We may then note the ionic conductivity of our sample and then read off the divalent-impurity concentration. Since the method of crystal purification is essentially purification by zone refining, we may expect that both the monovalent and the divalent impurity will be reduced and the divalent-impurity value obtained will represent a value somewhat smaller than the total impurity concentration.

Klemens[29] has predicted that random point defects should have a scattering rate

$$\tau^{-1} = \left(\frac{nV_0}{4\pi v^3}\right) \omega^4 \left\{ \left(\frac{\Delta M}{M}\right)^2 + 2\left[\frac{\Delta F}{F} - 13.44\left(\frac{\Delta R}{R}\right)^2\right] \right\}, \tag{23}$$

where n is the impurity concentration, V_0 is the unit cell volume, v is the average group velocity, ΔM is the mass difference between host and impurity atom, M is the average molecular mass, ΔF is the change in the force constant, and ΔR is the change in nearest-neighbor distance. Berman and Brock[14] have carefully confirmed both the proportionally constant $(\Delta M/M)^2$ and the functional form (ω^4) for isotopic phonon scattering in ^{6}LiF:^{7}LiF crystals. In the simplest approximation, phonons are scattered by chemical impurities in the same way as phonons are scattered by the random distribution of pure-crystal isotopic masses; that is,

$$\tau_I^{-1} = \frac{V_0}{4\pi v^3} \sum_i f_i \frac{\Delta M_i}{\overline{M}}^2 \omega^4, \tag{24}$$

where $\overline{M}$ is the average mass of the host lattice, ΔM the difference between the impurity mass and M, and f_i the fraction of unit cells having mass M_i. Since K^+ and Ca^{++} represent almost all of the impurity content, and since $\Delta M = 16$, 17, respectively, we need write only one expression for τ_I^{-1} whose coefficient will yield the fractional concentration of impurities in our crystals. Using the numbers from the ionic-conductivity results and the formula above, we have an explicit expression for the impurity-scattering rate:

$$\tau_I^{-1} = (1.6 \times 10^{-47}) \times (\text{ppm}) , \tag{25}$$

neglecting any force-constant changes. Finally, of course, this value must be put into the thermal-conductivity integrals and compared with experiment. Because the peak thermal conductivity is extremely sensitive to impurities in these very pure crystals, we should expect the fitted value, which includes both the mass-difference and the force-constant change scattering from all impurities, to be larger than the value calculated above.

B. Normal Process

Three phonon-momentum-conserving interactions (N processes) have been considered by Herring.[37] He has suggested that for a cubic crystal like NaF,

$$\tau_N^{-1} \propto \omega^n T^{5-n} , \tag{26}$$

where $n = 1$ for transverse phonons and $n = 2$ for longitudinal phonons. Furthermore, this form is expected to change to

$$\tau_N^{-1} \propto \omega^n T \tag{27}$$

at high temperatures. Phonon-transport measurements like the thermal conductivity of Fig. 2 not only average over all phonon polarizations, but extend across both the low- and high-temperature regions as well. For temperatures below about $16\,°K$, however, we are in the low-temperature region where a majority of the heat flow is composed of transverse phonons. In that case we should expect

$$\tau_N^{-1} = T_{N'} \omega \, T^4 . \tag{28}$$

We shall attempt to fit our thermal-conductivity data below $16\,°K$ using the previously determined relaxation rates along with τ_N^{-1} above. This fit will give us estimates of the scattering strength Γ_N. In Fig. 8 we have plotted the computed thermal conductivity for different impurity scattering strengths as well as for different N-process scattering strengths along with the experimental data. At low impurity concentration (curve A) we see that the N-process rate has relatively little effect. This is the effect of Eq. (3) mentioned before: For low concentration of impurities when N processes dominate, it is only the resistive scattering rate that affects
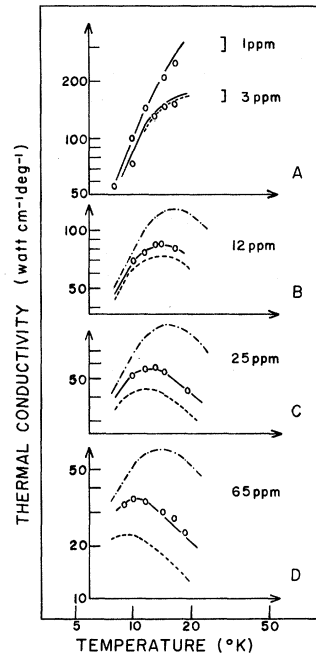
FIG. 8. Thermal conductivity vs temperature for varying N-process strengths and varying purity. The open circles are the experimental data for crystals of indicated impurity content. The N-process strengths illustrated are: dot-dashed lines, $\Gamma_N = 10^{-11}$; solid lines, $\Gamma_N = 10^{-10}$; dashed lines, $\Gamma_N = 10^{-9}$.

the computed thermal-conductivity curve. Curves B, C, and D show that a value of $\Gamma_N = 1 \times 10^{-10}$ generates curves in reasonable agreement with the data. A value of $\Gamma_N = 1 \times 10^{-11}$, for instance, is far too high and gives an incorrect temperature for the thermal-conductivity peak. A value of $\Gamma_N = 1 \times 10^{-9}$ is far too low and also gives an incorrect temperature for the thermal-conductivity peak. The uncertainty in the final strength is primarily the uncertainty in the impurity content of the crystals.

An attempt was also made to use the functional form $\tau_N^{-1} \propto \omega T^3$ to fit the data. The fit was slightly worse than $\tau_N^{-1} \propto \omega T^4$ and the latter was then used exclusively.

C. Umklapp Processes

We must now consider the intrinsic momentum-nonconserving phonon-phonon interaction – the U processes. By considering the number of phonons with the minimum wave vector necessary to undergo an umklapp collision, Peierls[10] showed that the U-processes rate must diminish with temperature as $e^{-\gamma \Theta / T}$, where γ is less than 1. A more complete analysis[38] suggested that

$$\tau_U^{-1} \propto \omega^2 T^3 e^{-\gamma \Theta / T} . \tag{29}$$

Krumhansl[39] has suggested, however, that

$$\tau_U^{-1} \propto \omega^2 T^2 e^{-\gamma\Theta/T} \qquad (30)$$

is probably more appropriate for NaF. The purer a crystal, the larger the temperature range where only the above U scattering dominates. In this temperature range, then, in the absence of the other resistive processes, one expects the thermal conductivity to vary exponentially. Can one determine the temperature dependence of the coefficient preceding the exponential term of the relaxation rate? Using the thermal-conductivity data from the best crystal, we have plotted KT^n vs $1/T$ on a semilog plot, Fig. 9, to attempt to obtain the coefficient. The exponential function is so strong, however, that
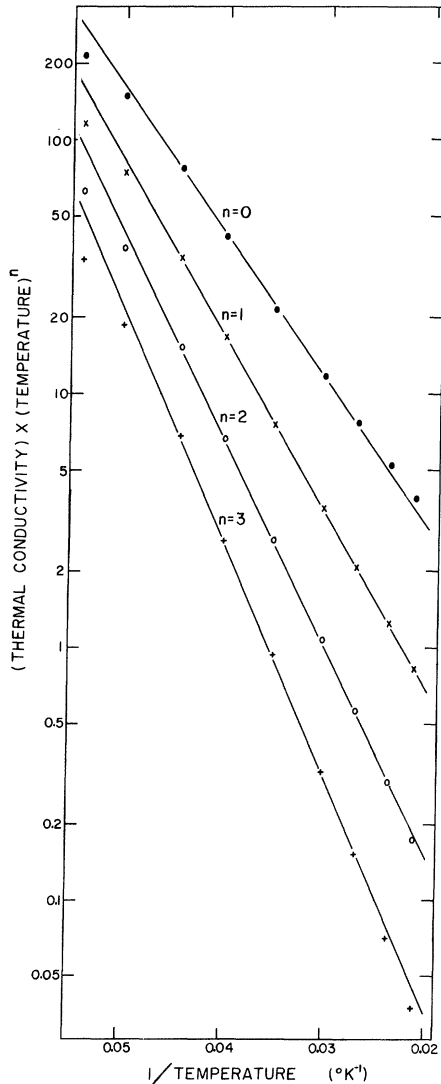

FIG. 9. Semilog plot of thermal-conductivity data for purest crystal times powers of temperature vs inverse temperature. Note the exponential form of the thermal-conductivity data.

varying n does not sharply affect a straight-line fit over a reasonable temperature region. We do see unequivocally that the thermal conductivity decreases exponentially with temperature over a wide range of temperatures — from about 20 to 35 °K. It might be noted that when significant ω^4 impurity scattering is present, a combination of impurity and U scattering produce a "flattened" TC curve which may yield an apparent but false exponential region.

With the relaxation time of

$$\tau_U^{-1} = \Gamma_U \, \omega^2 T^2 e^{-\gamma\Theta/T} \qquad (31)$$

we fit the thermal-conductivity curves directly since all the other relaxation times have been determined. The results for the best fit are shown in Fig. 10, with $\Gamma_U = 4.6 \times 10^{-20}$.

We note that the fit seems to fail badly above 40 °K. But remember that at higher temperatures, the scattering rates are expected to change. For high temperatures

transverse phonons: $\tau_N^{-1} \propto \omega T$ (Herring);

longitudinal phonons: $\tau_N^{-1} \propto \omega^2 T$,   (32)

while

$$\tau_U^{-1} \propto \omega^2 T \quad \text{(Krumhansl)}. \qquad (33)$$

For our "high"-temperature fit we have left the coefficient of the scattering strength the same and allowed the functional form to vary from the low-temperature form. The high-temperature forms no doubt evolve continuously from the low-temperature forms, but for the sake of simplicity we have normalized both forms at 37 °K and used the following high-temperature ones thereafter[40]:

$$\tau_N^{-1} \propto \omega T, \qquad (34)$$

$$\tau_U^{-1} \propto \omega^2 T/(e^x - 1). \qquad (35)$$

The final fit is seen in Fig. 11.

Equations (19), (22), (25), (28), (31), (34), and (35) represent the various phonon scattering rates for our purest crystal. Particular attention is drawn to Eqs. (28) and (34), which contain the N-process rates, and to Eqs. (19), (22), (25), (31), or (35), which can be added to give the total resistive scattering rate.

Now that a theoretical fit has been obtained, we may calculate a number of interesting quantities. It is instructive, if unreal, to let the coefficient of the impurity scattering term go to zero. The peak thermal conductivity then becomes 310 W/cm °K. If we then eliminate the physical imperfections, that is, the dislocation scattering, we obtain a peak thermal conductivity of 400 W/cm °K. So we have produced a crystal whose maximum thermal conductivity of 240 W/cm °K closely approaches the maximum intrinsically limited value. Further progress will require close attention not only to re-
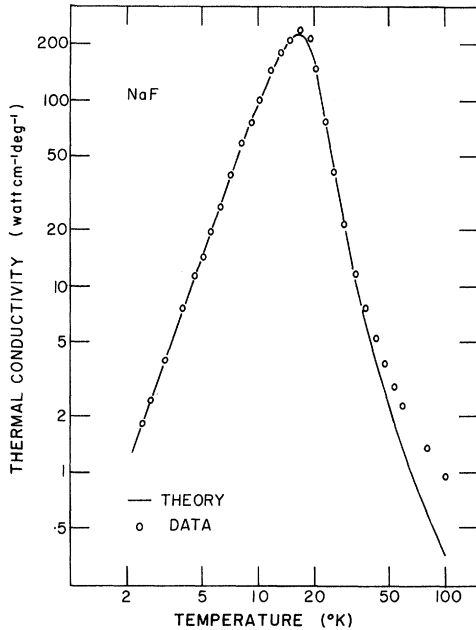
FIG. 10. Thermal conductivity of purest sample vs temperature: comparison of experimental data to the theory.

ducing the chemical impurities, but also to eliminating physical imperfections.

VI. DISCUSSION

To use the results of the thermal-conductivity analysis for examinations of the sound data, we construct a mean-free-path diagram using the re-
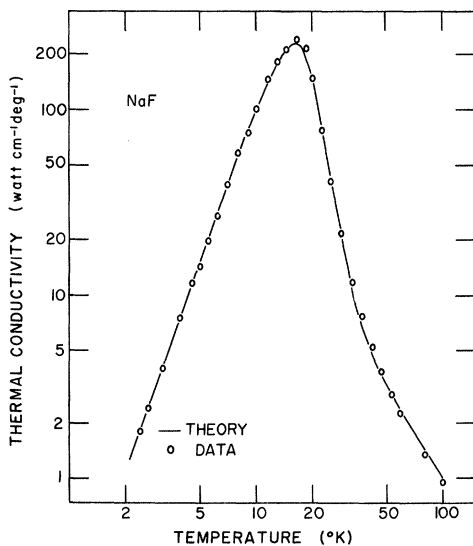

FIG. 11. Final fit of thermal-conductivity data using the full Callaway model and modified scattering terms above 37 °K.
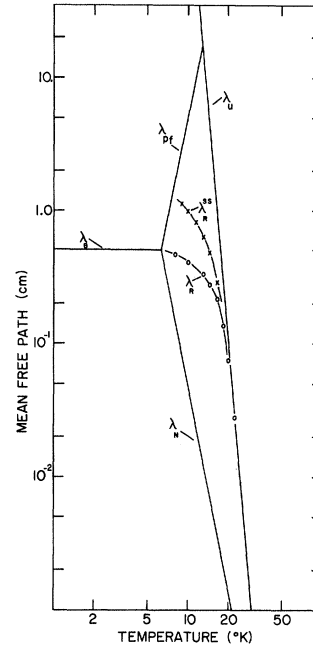

FIG. 12. Mean-free-path vs temperature diagram from thermal-conductivity analysis. λ_B, λ_{PE}, λ_U, and λ_N are the boundary scattering, Poiseuille-flow (see text), U-, and N-process mean free paths, respectively. λ_R is the total resistive mean free path for the thermal-conductivity sample. λ_R^{SS} is the resistive mean free path for a second-sound sample size (2×2 cm).

laxation times found above. We have averaged over the frequency dependences

$$\langle \tau \rangle = \int_0^\infty \tau \frac{x^4 e^x}{(e^x-1)^2} dx \Big/ \int_0^\infty \frac{x^4 e^4}{(e^x-1)^2} dx \qquad (36)$$

to obtain for the important N processes

$$\langle \tau_N^{-1} \rangle = 60 T^5 \ (\text{sec}^{-1}) \qquad (37)$$

and averaged similarly for the resistive processes to obtain

$$\langle \tau_U^{-1} \rangle = 2.2 \times 10^4 T^4 e^{-\Theta/3.5T} \ . \qquad (38)$$

The resultant diagram is shown in Fig. 12. λ_N is the N-process mean free path and λ_U is the U-process mean free path. λ_R represents the addition of all the resistive scattering in the best crystal.

We review the two essential conditions for second-sound propagation:

$$\lambda_N \ll d, \quad \lambda_R \gg \lambda_N, \qquad (39)$$

where d is the sample thickness. These conditions require that the N-process mean free path be much shorter than the sample thickness so that a macroscopic description is appropriate, and that the resistive-process mean free path be long compared to the N-process mean free path. That is, there must be a "window" in the mean-free-path diagram,

inside which second sound is possible. We note from the mean-free-path diagram that conditions seem favorable for second-sound propagation in our crystal over the region 10–25 °K.

Figure 6 showed the second-sound data for our best crystal. One sees that the "new" pulse first appears at 10 °K and becomes dominated by the diffusive flow at about 18 °K. In Fig. 5, similar behavior is seen for a crystal whose peak thermal conductivity is 150 W/cm °K. In this case, however, the second sound is dominated by the diffusive flow at about 14.5 °K. For a crystal whose peak thermal conductivity is 65 W/cm °K no second-sound pulse is seen at all.

In Table I we show values λ_R/λ_N for these three crystals of different purities, where the ratio is computed from the values of τ_R^{-1} and τ_N^{-1} obtained by computer fits to the thermal-conductivity data. In the table it is seen that $\lambda_R/\lambda_N > 1$ over a large temperature range. The heat-pulse data, however, suggest that the actual condition $\lambda_R/\lambda_N \gg 1$ is satisfied only above 10 °K, and only for the purest crystals since no second-sound pulse is seen for the $K_{\text{peak}} = 65$ W/°K cm crystal. Thus, the condition $\lambda_R/\lambda_N \gg 1$ is apparently not satisfied for $\lambda_R/\lambda_N = 4$, but is satisfied for $\lambda_R/\lambda_N \geq 10$. The second-sound sample size $d \sim 1$ cm can be compared with λ_N in Table I; it is seen that $\lambda_N < d$ at all temperatures.

Table II contains the values of λ_R used in computing λ_R/λ_N given in Table I. As can be seen, λ_R becomes of the order of 2 mm at 17 °K in the purest sample and at 11 °K in the least-pure sample. In order for the second-sound pulse to be detected the sample cannot be more than a few λ_R thick, or else the phonons will all have scattered out of the pulse. For realistic samples of 5–8-mm thickness, this means that if λ_R is less than about 2 mm, there will be no observed second sound, even if the λ_R/λ_N condition is satisfied. The second-sound pulse forms, at least in principle, but it never reaches the detector. This explains, for example, why second sound is not observed at 25 °K in our purest sample, even

though the λ_R/λ_N condition for second sound is satisfied as seen in Table I. Quantitatively, then, the inequalities allowing second-sound detection should read

$$\lambda_R/\lambda_N \geq 10, \tag{40}$$

$$\lambda_R \geq \tfrac{1}{4} d, \tag{41}$$

where d is the sample thickness.

The obvious solution when λ_R is short is to shorten the heat-pulse samples. We have done this and indeed the temperature to which one can follow the second-sound pulse is raised slightly. But since λ_R at high temperature is almost entirely due to U scattering, and that is decreasing λ_R exponentially, shorter crystals help only slightly.

One can also use the shape of the received second-sound pulses to deduce information on the various scattering lengths. Were we to draw a comparison to the solid ^{4}He data, we might judge the variation of the second-sound velocity observed here to be no more than temperature-dependent broadening – as N processes become scarcer for lower temperatures, not enough momentum-conserving collisions occur between the phonons to keep them in the temperature pulse. Thus, the pulse should broaden as temperature is decreased. An analysis of the pulse broadening as done by Ackermann and Guyer for solid ^{4}He would allow us to deduce λ_N as a function of temperature directly. However, inspection of Fig. 5 shows the second-sound pulses in NaF continuously broadening as the temperature is *increased*. If this is due to the N-process rate, we must conclude that N processes become less frequent as the temperature is increased, which is clearly not correct.

Lastly, we may examine the mean-free-path plot for the likelihood of Poiseuille flow of phonons. The criteria for this phenomenon are more stringent than for second-sound propagation, namely,

$$\lambda_N \ll R, \tag{42}$$

$$\lambda_R \gg \lambda_{PF} \equiv R^2/\lambda_N. \tag{43}$$

TABLE I. Ratio of resistive mean free path to N-process mean free path. Boundary scattering is excluded from λ_R because the samples are large ($\sim 2 \times 2$ cm).

Temp. (°K)	λ_N (mm)	1-ppm sample (second sound 10 – 18 °K)	6-ppm sample (second sound 10– 14 °K)	25-ppm sample (No second sound)
9.06	0.9	14	9.0	3.6
10.0	0.5	20	12	4.2
11.5	0.3	31	16	5.1
13.0	0.1	43	20	6.0
14.5	0.08	53	23	6.8
16.5	0.04	57	26	7.7
18.5	0.03	66	29	8.7
20.0	0.02	36	22	8.3
22.5	0.009	23	17	7.9
25.0	0.006	15	13	7.1

TABLE II. Resistive mean free path in cm vs temperature for several samples of different purities.

Temp. (°K)	1-ppm sample		6-ppm sample		25-ppm sample	
9.06		12		8.0		3.2
10.0		11		6.2		2.3
11.5	Second	8.3	Second	4.2	No	1.4
13.0	sound	6.2	sound	2.8	second	0.88
14.5	observed	4.5	observed	1.9	sound	0.58
16.5		2.5		1.1	observed	0.34
18.5		1.7		0.73		0.22
20.0		0.62		0.37		0.14
22.5		0.23		0.16		0.08
25.0		0.08		0.07		0.04

As can be seen by examination of the mean-free-path plot, the second condition is not met in our sample. Samples of smaller cross section would relax the second condition somewhat and might allow Poiseuille flow to be observed.

Note added in proof. An analysis of heat-pulse data in NaF, with an accompanying deduction of the various phonon scattering rates, has been done independently by Rogers [Phys. Rev. B (to be published)]. The difficulties with the temperature dependence of the pulse width [discussed briefly between Eqs. (41) and (42)] are clear in Roger's paper. His deduced values for τ_N^{-1} differ in some respects from ours. It should be borne in mind

that Rogers's analysis and ours start from very different points and attempt to converge on the same answer. He analyzed heat-pulse data directly to determine scattering rates. We analyzed thermal-conductivity data to determine scattering rates and then examined these rates to see if they were compatible with the observation of second sound.

ACKNOWLEDGMENTS

†Work supported by the Army Research Office, Durham, and by the Advanced Research Projects Agency through the Northwestern University Materials Research Center.

[1]J. Illukur and E. H. Jacobsen, in *Physical Acoustics*, edited by W. P. Mason (Academic, New York, 1968), Vol. V.

[2]For a general review of heat-pulse work, see R. J. von Gutfeld, in *Physical Acoustics*, edited by W. P. Mason (Academic, New York, 1968), Vol. V, p. 223.

[3]C. C. Ackermann, B. Bertman, H. A. Fairbank, and R. A. Guyer, Phys. Rev. Letters <u>16</u>, 789 (1966).

[4]C. C. Ackermann and W. C. Overton, Phys. Rev. Letters <u>22</u>, 764 (1969).

[5]T. F. McNelly, S. J. Rogers, D. J. Channin, R. J. Rollefson, W. M. Goubau, G. E. Schmidt, J. A. Krumhansl, and R. O. Pohl, Phys. Rev. Letters <u>24</u>, 100 (1970).

[6]Howard E. Jackson, Charles T. Walker, and Thomas F. McNelly, Phys. Rev. Letters <u>25</u>, 26 (1970).

[7]C. C. Ackermann and R. A. Guyer, Ann. Phys. (N.Y.) <u>50</u>, 128 (1968). This paper is an excellent review article on the subject of second sound.

[8]Matthey Bishop, Inc. Maluern, Pa. 19355.

[9]E. Merck, A. G., Darmstadt, Germany.

[10]R. E. Peierls, *Quantum Theory of Solids* (Clarendon, Oxford, 1955).

[11]T. F. McNelly and R. O. Pohl (private communication).

[12]J. Callaway, Phys. Rev. <u>113</u>, 1046 (1959).

[13]J. A. Krumhansl, Proc. Phys. Soc. (London) <u>85</u>, 921 (1965).

[14]R. Berman and J.C.F. Brock, Proc. Roy. Soc. (London) <u>A289</u>, 46 (1965).

[15]V. Peshkov, in *Report on the Cambridge Low Temperature Conference* (Physical Society, London, 1947), p.19.

[16]J. C. Ward and J. Wilks, Phil. Mag. <u>42</u>, 314 (1951); <u>43</u>, 48 (1952).

[17]E. W. Prohofsky and J. A. Krumhansl, Phys. Rev. <u>133</u>, A1403 (1964); R. A. Guyer and J. A. Krumhansl, *ibid.* <u>133</u>, A1411 (1964); <u>148</u>, 766 (1966); <u>148</u>, 778 (1966).

[18]C. P. Enz, Ann. Phys. (N.Y.) <u>46</u>, 114 (1968), and references therein.

[19]M. Chester, Phys. Rev. <u>131</u>, 2013 (1963).

[20]L A. Sussman and A. Thellung, Proc. Phys. Soc. (London) <u>81</u>, 1122 (1963); R. N. Gurzhi, Zh. Eksperim. i Teor. Fiz. <u>46</u>, 719 (1964) [Soviet Phys. JETP <u>19</u>, 490 (1964)].

[21]R. A. Guyer and J. A. Krumhansl, Phys. Rev. <u>148</u>, 778 (1966). The expression for the thermal conductivity in this reference allows for the possibility of Poiseuille flow. The Callaway expression does not, and could not be employed for analysis of data in which Poiseuille flow occurs.

[22]L. P. Mezhov-Deglin, Zh. Eksperim. i Teor. Fiz. <u>46</u>, 1926 (1964); <u>49</u>, 66 (1965); <u>52</u>, 866 (1967) [Soviet Phys. JETP <u>19</u>, 1297 (1964); <u>22</u>, 47 (1966); <u>25</u>, 568 (1967)]; W. D. Seward, D. Lazarus, and S. C. Fain, Jr., Phys. Rev. <u>178</u>, 345 (1969); E. M. Hogan, R. A. Guyer, and H. A. Fairbank, *ibid.* <u>185</u>, 356 (1969). For [3]He see William C. Thomlinson, Phys. Rev. Letters <u>23</u>, 1330 (1969).

[23]H. B. G. Casimir, Physica <u>5</u>, 495 (1938).

[24]Philip D. Thatcher, Phys. Rev. <u>156</u>, 975 (1967).

[25]G. A. Slack, Phys. Rev. <u>122</u>, 1451 (1961).

[26]M. G. Holland, Phys. Rev. <u>132</u>, 2461 (1963).

[27]R. Berman, E. L. Foster, and J. M. Ziman, Proc. Roy. Soc. (London) <u>A231</u>, 130 (1955).

[28]W. V. Houston, Rev. Mod. Phys. <u>20</u>, 161 (1948). Also see A. K. McCurdy, H. J. Maris, and C. Elbaum, Phys. Rev. (to be published).

[29]P. G. Klemens, Proc. Phys. Soc. (London) <u>A68</u>, 1113 (1955).

[30]P. Carruthers, Rev. Mod. Phys. <u>33</u>, 92 (1961).

[31]K. Ohashi, J. Phys. Soc. Japan <u>24</u>, 437 (1968).

[32]J. W. Davisson and Solomon Levinson, J. Appl. Phys. <u>38</u>, 4546 (1967).

[33]Analysis of Lot No. 060167 by E. Merck, A. G., Darmstadt, Germany.

[34]J. P. Harrison, G. Lombardo, and P. P. Peressini, J. Phys. Chem. Solids <u>29</u>, 557 (1968).

[35]C. F. Bauer and D. H. Whitmore, Phys. Status Solidi <u>37</u>, 585 (1970); and private communication.

[36]M. F. O'Brien and R. H. Plovnick, Mat. Res. Bull. <u>4</u>, 671 (1969).

[37]C. Herring, Phys. Rev. <u>95</u>, 954 (1954).

[38]P. G. Klemens, in *Solid State Physics*, edited by F. Seitz and D. Turnbull (Academic, New York, 1958), Vol. VII; G. Leibfried, in *Handbuch der Physik*, 2nd ed. (Springer-Verlag, Berlin, 1955), Vol. VII.

[39]As in Ref. 14.

[40]J. Krumhansl (private communication).